TECHNICAL NOTE

Radiation Medicine: Vol. 23 No. 5, 386–389 p.p., 2005

Ray Tracing Analysis of Overlapping Objects in Refraction Contrast Imaging

Masatsugu Hirano,[1] Katsuhito Yamasaki,[2] Hiroshi Okada,[3] Takashi Sakurai,[4] Takeshi Kondoh,[5] Tetsuro Katafuchi,[6] Kazuro Sugimura,[7] Sohei Kitazawa,[8] Riko Kitazawa,[8] Sakan Maeda,[8] and Shinichi Tamura[9]

We simulated refraction contrast imaging in overlapping objects using the ray tracing method. The easiest case, in which two columnar objects (blood vessels) with a density of 1.0 [g/cm^3], run at right angles in air, was calculated. For absorption, we performed simulation using the Snell law adapted to the object's boundary. A pair of bright and dark spot results from the interference of refracted X-rays where the blood vessels crossed. This has the possibility of increasing the visibility of the image.

Key words: synchrotron radiation, refraction contrast, ray tracing method, overlapping objects

Introduction

It is difficult to observe objects that have a small absorption difference using conventional absorption imaging, in spite of the rapid development of X-ray diagnostic devices. The practical application of a coherent X-ray source like laser is expected in the next generation. Refraction contrast imaging using highly coherent X-rays (synchrotron radiation) produces images that reflect objective density difference and have the possibility of clinical application. This imaging produces a bright/dark line pair at the object's boundary and has the effect of increasing visibility.[1-3] However, quantitative analysis of this imaging has not been carried out. Conventional sources have less coherence and are not able to produce such high-quality images. In this paper, refraction contrast imaging of crossing objects is simulated using the ray tracing method.[4] This paper assumes the existence of pillars with a density equal to water in air, for simplification of the X-ray imaging simulation.

Materials and Methods

The refraction index for X-rays is usually expressed as $n=1-\delta+i\beta$, where both δ and β are very small. δ is proportional to the density and square of the wavelength. For example, in water, δ is 2.3×10^{-7} and β is 1.2×10^{-10} at 30 keV. Therefore, the refraction index is much larger than the index of absorption. The real part of the refractive index is smaller than but close to 1.0. Therefore, the refraction angle is small. In Fig. 1, the refraction angle is 0.23 μrad (in the case of an incident angle of 45 degree).

Monte Carlo Simulation was applied to calculation of the travel paths of X-rays along the object surfaces, and absorption is considered in this paper. The number of photons radiated into the pixels of each detector was counted, and the number of counts was interpreted as intensity. Direction of X-ray at the margin of objects is calculated by the Snell law. This simulation program was originally developed by us. The program is described by C language.

The conditions were as follows in the calculation of ray tracing. The 30 keV monochromatic X-ray was exposed in air to the part at which two same-size pillars (diameter of 100 micrometers), assumed to be blood vessels with a density equal to 1.0 [g/cm^3], intersected at right angles (Fig. 2). The refraction contrast image

Received September 22, 2003; revision accepted September 25, 2004.

[1]Niihama National College of Technology
[2]Japan Synchrotron Radiation Research Institute
[3]Department of Urology, Teikyo University School of Medicine
Departments of [4]Internal and Geriatric Medicine, [5]Neurosurgery, [7]Radiology, and [8]Pathology, Kobe University Graduate School of Medicine
[6]National Cardiovascular Center
[9]Osaka University Graduate School of Medicine
Reprint requests to Masatsugu Hirano, Ph.D., Niihama National College of Technology, 7-1 Yagumo, Ehime 792-8580, JAPAN.

This work has been performed under the approval of the Photon Factory Program Advisory Committee (Proposal No. 2003P010).

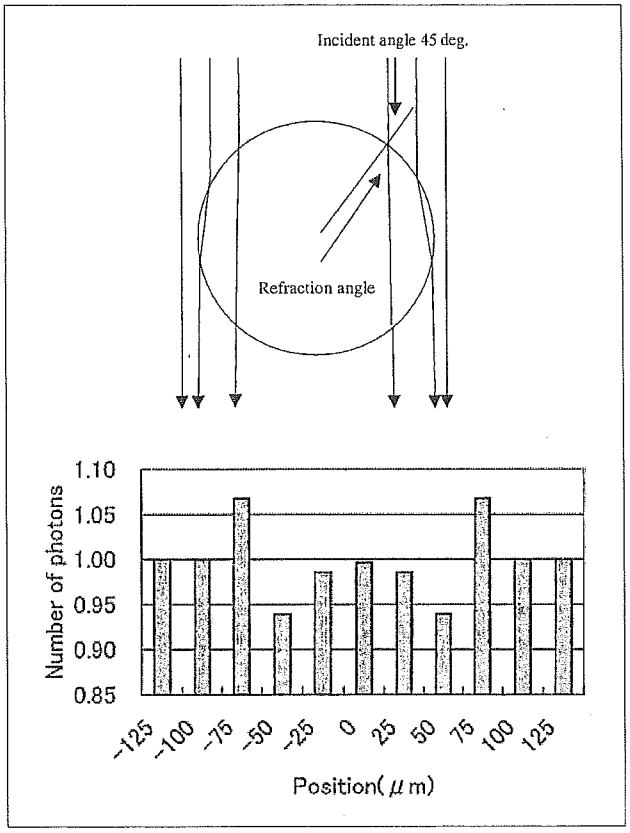

Fig. 1
A: Refraction contrast imaging. Parallel X-ray beams are bent by refraction, generating bright and dark lines outside and inside the boundary lines, respectively.
B: Profile curve of 30 keV X-ray refraction by pillars with a diameter of 100 μm (specific density = 1.0) observed with a detector in the case of a pixel size of 25 μm (the background is normalized to 1.0). Vertical numbers are photon counts into detector.

A
B

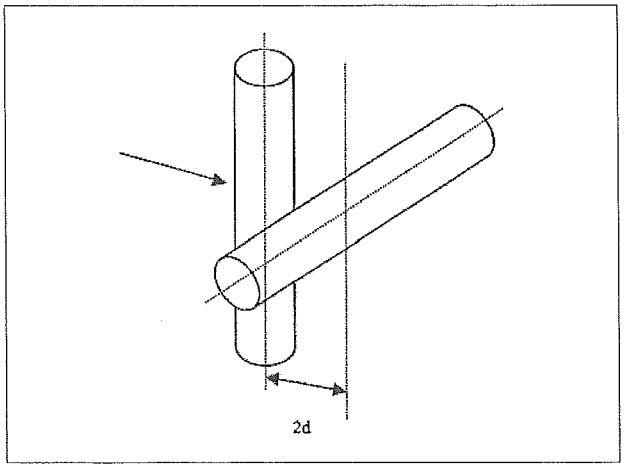

Fig. 2. Spatial relationship of two columns (diameter: d).

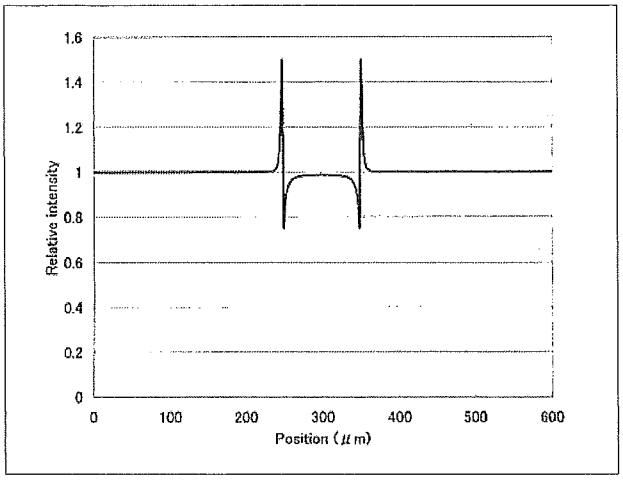

Fig. 3. Profile curve of the refraction image of a 100 μm cylinder.

was obtained 1[m] behind the sample. The ray tracing method was used in calculating parallel X-rays running at the surface of objects (Fig. 1). Finally, photons incident to each pixel (pixel size, 1 micrometer) of the detector were counted, and the number of counts was expressed as the intensity of the pixel. Then the simulated image was compared with the observed image. The experimental conditions were as follows. A plastic fiber with a diameter of 0.5 mm was scanned with a nuclear plate, applying 30 keV monochrome X-rays at BL-14C in PF-KEK.

Results

The profile of the refraction contrast image is shown in Fig. 3 (single 100 [μm] cylinder), and the calculated images of the two columns are shown in Fig. 4A-1. It can be observed that pairs of bright and dark lines are produced in the boundary area, and the brightest/darkest spots come from overlap of bright/dark lines (magnified in Fig. 4B). The observed image of crossed glass fiber (500 μm) using an analyzer crystal at 30 keV is shown in Fig. 5. The distance between the nearest fiber and detector was 1.0 mm. The distance between two fibers was 2.0 mm. A simulated image of crossed fibers obtained using an analyzer crystal is shown in Fig. 6. The two images show good coincidence. The profile curves of observed and simulated images of two crossed fibers are shown in Fig. 7.

Discussion

X-ray beams apparently refract at the boundary of objects. The contrast between the bright line produced at the low specific gravity side (air) and the dark line at the high specific gravity side (blood vessels) is much

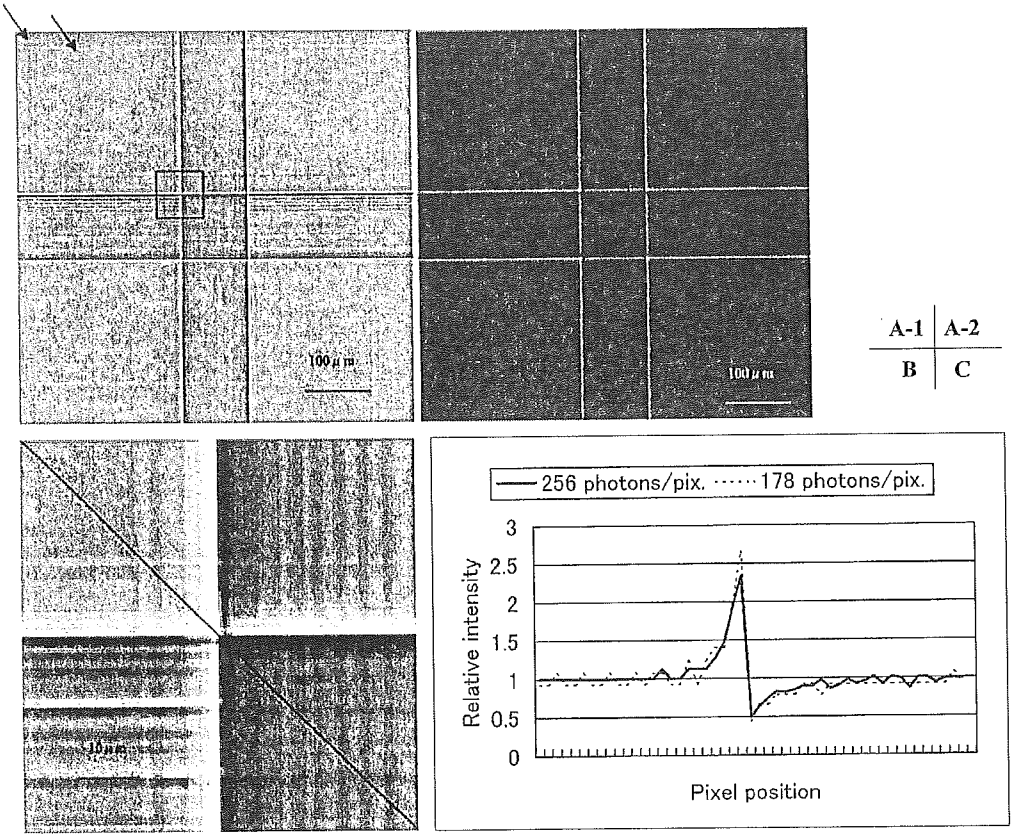

Fig. 4
A-1: Refraction image (256 photons/pix.) of two crossed 100 μm cylinders. *Arrows* show artifact pattern (vertical and horizontal lines) due to discontinuity.
A-2: Refraction image (178 photons/pix.) of two 100 μm cylinders.
B: Magnified image of the rectangular area in Fig. 4A.
C: Solid diagonal line profile of Fig. 4B.

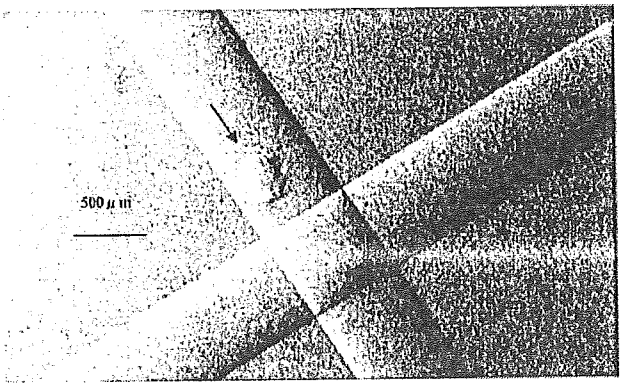

Fig. 5. Image of crossed glass fibers (500 μm) using analyzer crystal at 30 keV. *Arrow* shows debris.

larger than that of absorption. The overlap of the above-mentioned contrast generates the contrast-enhanced border spots due to the additional enlargement of contrast.

Under the condition of this simulation, the contrast of the brightest spot compared with the darkest spot that was produced by the overlapping of two fibers was 1.6 times larger than the contrast of the light-and-dark line at the margin of the obstacle (Figs. 3, 4C), and has the potential to be clearly useful for diagnostic ability. However, there is a possibility of interfering with diagnosis. Many bright and dark spots are produced in the

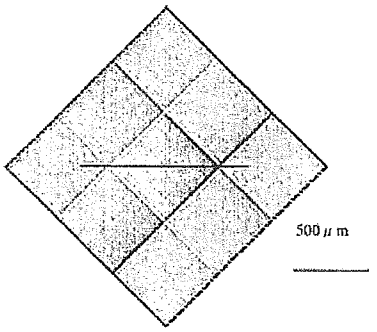

Fig. 6. Simulated image of crossed fibers obtained using an analyzer crystal. The two images show good coincidence at 30 keV.

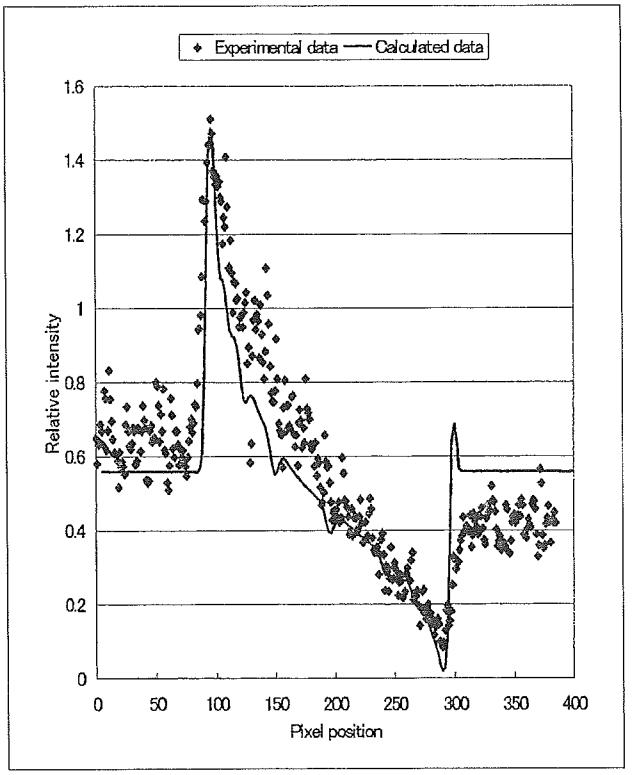

Fig. 7. Profile curves of observed and simulated images (solid line profile of Fig. 6).

case of many overlapping vessels. Further, small ringing artifact is observed in Fig. 4C due to discontinuity of the calculation. The artifact is regarded as digital noise that results from digitizing photon counts at each pixel of the detector. A simulated image is shown in Fig. 4A-1. Photon numbers are 256 at one pixel in Fig. 4A-1. A simulated image is shown in Fig. 4A-2, and photon numbers are 178 in this image. A profile curve is shown in Fig. 4C. For the same reason, the horizontal column in Fig. 4A-1 has the artifact pattern at the boundary area. For example, the ratio of vertical line intensity shown by the arrow to background intensity is 1.0625 in Fig. 4A-1.

Although the interference caused by the overlap of objects can be simulated with the Maxwell equation, the calculation performed in this study may be a good calculation method as a primary approximation of the Maxwell equation.[4] Simulation of and experimentation on X-ray absorption and interference by multiple-objects have just started, and more study is needed. The ray tracing method is useful as calculation tool for the above-mentioned simulation, and we will continue further research.

References

1) Snigirev A, Snigireva I, Kohn V, *et al.* On the possibilities of x-ray phase contrast micro-imaging by coherent high-energy synchrotron radiation. *Rev Sci Instrum*, 66: 5486–5492, 1995.
2) Yagi N, Suzuki Y, Umetani K, Kohmura Y, Yamasaki K. Refraction-enhanced x-ray imaging of mouse lung using synchrotron radiation source. *Med Phys*, 26: 2190–2193, 1999.
3) Yamasaki K, Hirano M, Nagai H, *et al.* Refraction-enhanced X-ray imaging using synchrotron radiation source. *TECHNICAL REPORT OF IEICE*, MI2001–46: 15–20, 2001.
4) Stam J, Languenou E. Ray tracing in non-constant media. In *7th EUROGRAPHICS Workshop on Rendering*, (Springer-Verlag), 1996.

Diabetes/Metabolism Research and Reviews -

Cognitive dysfunction associates with white matter hyperintensities and subcortical atrophy on magnetic resonance imaging of the elderly diabetes mellitus Japanese Elderly Diabetes Intervention Trial (J-EDIT)

Journal:	*Diabetes/Metabolism Research and Reviews*
Manuscript ID:	DMRR-05-RES-115.R1
Wiley - Manuscript type:	Research Article
Date Submitted by the Author:	16-Nov-2005
Complete List of Authors:	Akisaki, Taichi; Kobe university graduate school of medicine, Internal and geriatric medicine Sakurai, Takashi; Kobe University Graduate School of Medicine, Internal and Geriatric Medicine Takata, Toshihiro; Kobe University Graduate School of Medicine, Internal and Geriatric Medicine Umegaki, Hiroyuki; Nagoya University Graduate School of Medicine, Geriatrics Araki, Atushi; Tokyo Metropolitan Geriatric Hospital, Endocrinology Mizuno, Sachiko; Tokyo University, Biostatistics / Epidemiology and Preventive Health Sciences, School of Health Sciences and Nursing Tanaka, Shiro; Tokyo University, Biostatistics / Epidemiology and Preventive Health Sciences, School of Health Sciences and Nursing Ohashi, Yasuo; Tokyo University, Biostatistics / Epidemiology and Preventive Health Sciences, School of Health Sciences and Nursing Iguchi, Akihisa; Nagoya University Graduate School of Medicine, Geriatrics Yokono, Koichi; Kobe University Graduate School of Medicine, Internal and Geriatric Medicine Ito, Hideki; Tokyo Metropolitan Health and Treatment Corporation, Tama-Hokubu Medical Center
Keyword primary:	Type 2 diabetes mellitus, Subcortical atrophy, White matter hyperintensities, Periventricular hyperintensity, Cognitive dysfunction, Elderly

Cognitive dysfunction associates with white matter hyperintensities and subcortical atrophy on magnetic resonance imaging of the elderly diabetes mellitus

Japanese Elderly Diabetes Intervention Trial (J-EDIT)

A short title
Diabetic cognitive dysfunction (J-EDIT)

Taichi Akisaki[1], Takashi Sakurai[1]*, Toshihiro Takata[1], Hiroyuki Umegaki[2], Atsushi Araki[3], Sachiko Mizuno[4], Shiro Tanaka[4], Yasuo Ohashi[4], Akihisa Iguchi[2], Koichi Yokono[1] and Hideki Ito[5]

[1] Department of Internal and Geriatric Medicine, Kobe University Graduate School of Medicine, Kobe, Japan

[2] Department of Geriatrics, Nagoya University Graduate School of Medicine, Aichi, Japan

[3] Department of Endocrinology, Tokyo Metropolitan Geriatric Hospital, Tokyo, Japan

[4] Department of Biostatistics / Epidemiology and Preventive Health Sciences, School of Health Sciences and Nursing, Tokyo University, Tokyo, Japan

[5] Tokyo Metropolitan Health and Treatment Corporation, Tama-Hokubu Medical Center

*Correspondence: Takashi Sakurai
Department of Internal and Geriatric Medicine
Kobe University Graduate School of Medicine
7-5-1 Kusunoki-cho, Chuo-ku, Kobe 650-0017, Japan
E-mail: taichi@med.kobe u.ac.jp Tel. +81 78 382 5901 FAX +81 78 382 5919

Abstract

Background. Type 2 diabetes mellitus is associated with cognitive dysfunction and increases the risk for dementia in the elderly. The aim of this study was to explore, by means of magnetic resonance (MR) imaging, possible relationships among clinical profiles of diabetes, cognitive function, white matter hyperintensities (WMHs) and subcortical brain atrophy.

Methods. Data were obtained from 95 non-demented type 2 diabetic participants aged 65 years or over, enrolled in an intervention trial for Japanese elderly diabetics. Cognitive function was measured with neuropsychiatric tests, including mini-mental state examination (MMSE , verbal memory, digit symbol substitution and Stroop tests. Hyperintensity was classified into periventricular, deep white matter, thalamic and basal ganglia. Four ventricle-to-brain ratios were used to measure subcortical atrophy. To identify clinical features of diabetes, indices of glycemic control, lipid metabolism, blood pressure and complications were examined. Canonical correlation analysis and regression analysis were used to assess correlation.

Results. Score for digit symbol substitution and MMSE negatively correlated with WMHs in parietal lobe and hyperintensities in thalamus, respectively. Lower scores for memory and digit symbol substitution showed positively association with enlarged subcortical atrophy adjacent to lateral ventricles. There was no association between clinical pictures of diabetics with cognitive dysfunction and of those with morphological changes in the brain.

Conclusions. Impaired cognitive domains of speed of mental processes and memory were associated with WMHs and subcortical atrophy. Degenerative

changes in cerebral small vessels may constitute predictive factors for the rate of cognitive dysfunction in elderly diabetics.

Keywords: Type2 diabetes mellitus, Elderly, Cognitive dysfunction, Periventricular hyperintensity, White matter hyperintensities, Subcortical atrophy.

Introduction

Type 2 diabetes is an age-related disease with a prevalence in Japan estimated at more than 5 percent of the population (1). For elderly diabetics, the purpose of treatment is not only to control plasma glucose levels, but also to prevent diabetic complications. Prospective intervention studies have provided evidence that intensive glycemic control effectively slows the onset and progression of diabetic vascular complications associated with type 2 diabetes (2). However, these epidemiological investigations did not consider the various aspects to prevention of cognitive decline in elderlydiabetics.

The influence of diabetes on brain function has been of interest for more than 80 years (3, 4). Subjects with type 2 diabetes initially manifest deficits in abstraction, problem solving, memory and the completion of tasks involving speed and complex perceptual-motor responses. Recently, several epidemiological studies have shown that diabetes increases the risk for the most common forms of dementia, Alzheimer's disease and vascular dementia (5-9). Hence, the most critical issue is to identify the factors responsible for diabetic cognitive impairment that lead to severe cognitive decline in the elderly. Diabetes-related brain disorders have been considered multifactorial and attributed to genetic predisposition, nutritional factors, cerebrovascular disorders, and the neurotoxic effects of hypoglycemia and hyperglycemia (10). The so-called Rotterdam study, which is one of the largest population-based cohort studies, demonstrated conclusively that diabetic subjects with cerebrovascular diseases and with insulin treatment are more prone to dementia (5). Recent biological findings have supported the view that several

risk factors could be linked between diabetes and cognitive dysfunction in the elderly (10; 11). However, clinical pictures of elderly diabetes are various and elderly diabetics may have oincident neuropsychiatric disorders, thus making it difficult to identify the factors specifically responsible for cognitive decline.

To address these controversies regarding cognitive decline in elderly diabetics, we conducted a large-scaled prospective study of the Japanese Elderly Diabetes Intervention Trial (J-EDIT). J-EDIT was a prospective intervention study designed to investigate and identify the clinical characteristics of non-demented diabetic elderly. In the report presented herewe have analyzed the baseline measures of cognitive dysfunction in non-demented elderly with type 2 diabetes. The aim of this study was to explore possible associations among diabetic cognitive dysfunction, brain morphological changes detected on magnetic resonance (MR) imaging, and diabetic clinical features. To analyze brain MR images, we focused on white matter hyperintensities (WMHs) and subcortical brain atrophy because subcortical structural changes have been associated with cognitive impairment in demented and nondemented elderly subjects (12, 13). We classified hyperintensities into periventricular, deep white matter, thalamic and basal ganglia. The research questions were: 1) What diabetic indices are associated with cognitive dysfunction? : 2) Which WMHs influence specific cognitive domains of elderly diabetics? : 3) Do brain structural changes on MR imaging correlate with clinical measurements of diabetes? To address these questions, we adopted the canonical correlation analysis and regression analysis.

Materials and Methods

Participants: J-EDIT started in 2001 as a prospective intervention study of Japanese elderly with diabetes mellitus to prevent the several diabetic complications. The study involved 1,173 diabetic subjects from 42 institutes and hospitals in Japan who were 65 years or older (mean age was 71.8 ± 4.6) and whose serum HbA1c levels were ≧ 7.0%. Written informed consent was obtained from all patients. From these subjects enrolled in the J-EDIT we selected 95 subjects with type 2 diabetes (14), who were treated at Kobe University Hospital, Nagoya University Hospital, Chiaki Hospital, Aoki Memorial Hospital, Nagoya Kyoritsu Hospital and Tokyo Metropolitan Geriatric Hospital. The diabetic participants who had difficulties in communicating, or showed signs of speech disturbance, deafness, severe disturbance of visual acuity, dementia, and serious deterioration of the activities of daily life were excluded from this study. Clinical diagnosis of dementia was established according to the criteria of the Diagnostic and Statistical Manual of Mental Disorders (DSM)-IV (15). Subjects with chronic renal failure (serum creatinine > 1.5 mg/dl), serious heart failure or symptomatic cerebral infarctions were alsoexcluded from this study.

Assessment of diabetes mellitus, complications, and comorbidities: The diagnosis and information of diabetes mellitus, blood examinations and complications were obtained from clinical charts (14). Blood samples were obtained by vein puncture after overnight fasting to assess serum levels of glucose, HbA1c, total cholesterol, triglyceride, and HDL-cholesterol. Serum insulin concentrations were measured in patients who were not receiving insulin therapy. Diabetic vascular complications were assessed for the co-existence of

nephropathy, retinopathy, neuropathy and coronary diseases. Retinopathy was assessed fundoscopically through the dilated pupils by experienced ophthalmologists. The degree of retinopathy was classified into five categories; 0 (no retinopathy), 1 (intra-retinal hemorrhages and hard exudates), 2 (soft exudates), 3 (intra-retinal microvascular abnormalities, venous calibre abnormalities and venous beading), 4 (neovascularization of the disc or elsewhere in the retina, preretinal fibrous tissue proliferation, preretinal or vitreous hemorrhage, and retinal detachment). Nephropathy was assessed in terms of the mean urinary albumin-to-creatinine ratio (ACR) and rated as 1 (no nephropathy: ACR<30 μg/mg), 2 (microalbuminuria: 30≦ ACR< 300 μg/mg), or 3 (persistent proteinuria: ACR≧ 300 μg/mg or urinary protein≧ 30 mg/dl). Diabetic neuropathy was classified as 1 (no neuropathy), 2 (loss of Achilles tendon reflex without neuropathic symptoms including paresthesia), or 3 (neuropathic symptoms). Coronary artery diseases were considered to be present when diabetic patients had at least one of the following: a history of myocardial infarction characterized by a typical clinical picture (chest pain, chest oppression, dyspnea, typical changes on ECG accompanied by pathological Q waves and/or localized ST variations), and typical enzymatic changes. Cardiovascular complications were classified into two categories, that is, presence or absence of coronary artery diseases.

Clinical diagnosis of hypoglycemia was based on the modified Whipple triad: symptoms and/or signs consistent with a low glucose concentration, low plasma glucose concentrations (< 60 mg/dl), and relief of symptoms associated with restoration of plasma glucose level (16). Subjects with at least one

hypoglycemic episode during the recent twelve months were considered to have hypoglycemia.

Procedures for analysis of the brain MR imaging: For every diabetic subject, a series of axial standard T1-weighted (repetition time [TR], 400msec; echo time [TE], 12msec), T2-weighted (TR, 3000msec; TE, 90msec; a 256 x 512 matrix) and fluid-attenuated inversion-recovery (FLAIR) (TR, 7500msec; TE 110msec; inversion time, 2200msec; a 256 x 512 matrix) MR sequences of the brain were performed using 1.5 Tesla MR units (Gyroscan NT-Intera and Gyroscan ASC-NT, both Philips, Eindhoven, The Netherlands; SIGUMA MR/I, General Electric, Milwaukee, WI). Scans in parallel with the anterior commissura—posterior commissura line were performed from the vertex to the foramen magnum with 7 mm-thick slices and an inter-slice gap of 1.4 mm.

We analyzed WMHs and subcortical brain atrophy on MR images. WMHs appeared as hyperintense on T2-weighted images, but did not leave a clear hypointense hole on T1-weighted images (Figure 1a). FLAIR was used to obtain a clearer picture of the various WMHs (17), which were classified into subcortical WMHs and periventricular hyperintensity (PVH) (Figure 1b). WMHs were considered periventricular if the largest diameter was adjacent to the ventricular lining; otherwise, they were considered subcortical. PVH was rated semiquantitatively as 0 (none), 1 (pencil thin lining: <3 mm from the edge of ventricles), 2 (smooth halo: 3-10 mm), 3 (extending cap or thick lining: 10-25 mm), 4 (large confluent: >25 mm) for three separate regions; adjacent to frontal horns (frontal caps), adjacent to the wall of the lateral ventricles (bands), and adjacent to the occipital horns (occipital caps). The overall degree of PVH was

calculated by adding up the scores for the three separate compartments (range 0-24) (18, 19). The number and size of subcortical WMHs were counted in the frontal, parietal, occipital, and temporal lobes, as were the number and size of hyperintensities in the basal ganglia and thalamus. The size of subcortical WMHs was classfied, according to the largest diameter, that is, small (1-3 mm), medium (3-10 mm), or large (>10 mm) (17). To calculate the volume of subcortical hyperintensities they were assumed to be spherical with a fixed diameter of 2, 6, 12 mm for each of the three respective categories.

Linear analysis of subcortical brain atrophy, Evans Ratio (ER), inverse Cella Media Index (iCMI), Caudate Head Index (CHI), and Basal Cistern Index (BCI) were all calculated (20-23). The following were measured with slide calipers: the maximum distance between the tips of the anterior horns (A), the width between the bilateral heads of the caudate nuclei (B), the maximum transverse inner diameter of the intracranial space (C) , the maximum width of the cella mediae (D) and the maximum transverse inner diameter (E). Finally, the internal width between the bilateral temporal lobe (F) and the maximum transverse inner diameter (G) were calculated. The CHI, iCMI, ER and BCI were calculated with the following respective formulae: CHI=B/C, iCMI=D/E, ER=A/C and BCI=F/G, respectively (Figure 2).

Two raters who had no knowledge of the clinical data analyzed the brain MR imaging. To test the interrater reliability, the result of the two raters was subjected to correlation analysis for comparison in a random sample of 15 subjects. The analysis showed a strong correlation ($r=0.85–0.89$, $P<0.0001$),

which suggested that the method of measurement used for this study was reliable.

Measurement of Cognitive Function: We used neuropsychiatric test batteries to examine cognitive function of each of the subjects by assessing the speed of cognitive processes, as well as the extent of verbal memory, and global cognitive function. Two tests were used to assess the speed of mental processes: Stroop B (naming the color of the character that was printed in a color other than the one signified by the characters) and the digit symbol substitution test of the Wechsler Adult Intelligence Scale-Revised (24, 25). Verbal memory was assessed with the immediate and delayed word-list recall from the logical memory subtest of the Alzheimer's Disease Assessment Scale and of the paragraph from the neuropsychological tests of the National Center of Neurology and Psychiatry, Japan (26, 27). Finally, MMSE was used to measure global cognitive function (28).

Statistical analysis: To explore the association among cognitive profile, clinical variables of diabetes, and morphological changes in MR imaging, we used canonical correlation analysis and regression analysis (29). There were four sets of variables: seven cognitive tests, sixteen clinical variables of diabetes, eight brain WMH regions and four indices of brain atrophy. Since multiple test corrections would wipe out virtually any test significance, and variables within the same class are often showed a high degree of correlation, thus rendering the correlations redundant, we adopted the canonical correlation analysis to identify the direct relationship between two sets of variables. The fundamental principle behind canonical correlation analysis is creation of a number of

canonical solutions, each consisting of a linear combination of one set of variables, which has the form:

$U_i = a_1\,(predictor_1) + a_2\,(predictor_2) + \cdots + a_m\,(predictor_m)$

and a linear combination of the other set of variables, which has the form:

$V_i = b_1\,(criterion_1) + b_2\,(criterion_2) + \cdots + b_n\,(criterion_n)$

The purpose is to determine the coefficients (a's and b's) that maximize the correlation between canonical variates U_i and V_i. The first canonical correlation is the highest possible correlation between any linear combination of the variables in the predictor set and any linear combination of the variables in the criterion set.

A way of interpreting the canonical solutions is to look at the correlations between the canonical variates and the variables in each set. These correlations are called structure coefficients. The logic here is that variables that are highly correlated with a canonical variate have more in common with it and they should be considered more important when deriving a meaningful interpretation of the related canonical variates. As a substantial value of structure coefficients, an absolute value equal to or greater than 0.3 is often used (30, 31).

For adjustment for confounders such as age and education, the correlation between cognitive function and MRI findings detected by the canonical correlations analysis was reanalyzed with multiple linear regression analysis. Statistical significance was defined as $p < 0.05$.

Results

Clinical characteristics of the 95 elderly diabetic patients are shown in Table 1. The mean age of the patients and duration of diabetes mellitus were 72.8±0.5 years and 18.4±1.2 years, respectively. Average HbA1c was 7.9±0.1%, while other indices, such as blood pressure, serum cholesterol level and body mass index, were within reasonable limits. Eighteen diabetic subjects were receiving insulin therapy and 21 patients had hypoglycemic episodes. Because the number of patients in this study with insulin treatment or with hypoglycemic episodes was small, we could not analyse the effect of insulin therapy or hypoglycaemia on cognitive dysfunction.

Canonical correlation analysis indicated a strong association of cognitive function with WMHs (p=0.004) (Table 2). The canonical valuable of WMHs was contributed with digit symbol substitution test, MMSE, immediate/delayed word-list recall, and Stroop tests (correlation of canonical variables: 0.76, 0.65, 0.33, 0.47, -0.41, respectively) and the canonical valuable of cognitive function was contributed with PVH and WMHs in the parietal, temporal and occipital lobes, total WMHs, and hyperintensities in the thalamus (correlation of canonical variables: -0.45, -0.33, -0.31, 0.33, -0.34, -0.39, respectively), but not with WMHs in frontal lobe. In other words, digit symbol substitution test, MMSE and immediate/delayed word-list recall had a negative correlation with PVH and with WMHs in the parietal and temporal lobes, total WMHs and hyperintensities in the thalamus and positive correlation with WMHs in the occipital lobe. These results suggest that diabetic patients with more predominant WMHs except in

the frontal lobe were more deficient in speed of mental proesses and in verbal memory.

The relationship between cognitive function and clinical indices was analyzed. No correlation could be established between cognitive function and clinical indices of diabetes, including glycemic control, lipid metabolism, blood pressure and complications of diabetes mellitus (data not shown). There was no correlation between WMHs and diabetic clinical pictures including diabetic control and complications (data not shown).

Table 3 shows a clear correlation of diabetic cognitive dysfunction with subcortical brain atrophy indices ($p=0.004$). Lower scores for word-list recall and digit symbol substitution test, as well as delayed paragraph recall were positively associated with enlarged ER, CHI and iCMI. Canonical correlation did not detect a significant association between brain atrophy and diabetic clinical indices (data not shown).

The results were reanalyzed with regression analysis to adjust for age, education and systolic blood pressure, because these factors were generally considered to have effects on the cognitive function and/or brain structural changes on MR images (32, 33). The variables which strongly contributed to the canonical variates between cognitive functions and MRI findings were selected as the criterion variables of the regression analysis. In these analyses, digit symbol substitution test was associated with WMHs of parietal lobe, and MMSE was correlated with hyperintensities in the thalamus after adjustment for age, education, and systolic blood pressure (Table 4). Table 5 shows the significant relationship between immediate word-list recall and caudate head index and the

association between digit symbol substitution test and inverse cella media index.

Discussion

The study presented here represents the first investigation analyzing the possible associations between cognitive dysfunction and clinical features, with simultaneous evaluation of brain morphological changes detected on MR images in nondemented elderly with type 2 diabetes. It was found that WMHs and subcortical brain atrophy strongly correlate with several domains of diabetic cognitive impairment, such as impaired speed of cognitive processes and memory. Our study also indicates that the various and separate subcortical hyperintensities in the parietal lobes and in the thalamus, but not in the frontal lobe, are associated with diabetic cognitive impairment. However, we could not detect the diabetic factors responsible for cognitive dysfunction, nor for the morphological changes on MR images, in spite of our thorough investigation of the various diabetic indices, including diabetic control, complications and comorbidities. These findings were established with the canonical correlation analysis used for our study.

Previous studies have investigated the relationship between WMHs and cognitive decline in non-demented and demented elderly (18, 34-38). Cognitive test scores in older adults were found to be worse in the presence of severe WMHs, even after adjustments for age, gender and education (18). PVH is more likely than subcortical WMHs to be associated with speed of cognitive processes and memory (18, 34, 35). The white matter of the subcortical